Turbulence Structure in the Convective Boundary Layer

J. C. KAIMAL,[1] J. C. WYNGAARD,[2] D. A. HAUGEN,[1] O. R. COTÉ AND Y. IZUMI

Air Force Geophysics Laboratory, Hanscom AFB, Mass. 01731

S. J. CAUGHEY AND C. J. READINGS[3]

Meteorological Research Unit, RAF Cardington, Bedford, England

(Manuscript received 23 March 1976, in revised form 16 July 1976)

ABSTRACT

Results from a boundary layer experiment conducted over a flat site in northwestern Minnesota are discussed. Wind and temperature fluctuations near the ground were measured with AFCRL's fast-response instrumentation on a 32 m tower. Measurements between 32 m and the inversion base z_i were made with MRU probes attached at five different heights to the tethering cable of a 1300 m³ kite balloon. The daytime convective boundary layer appears to be well-mixed with evidence of significant heat and momentum entrainment through the capping inversion.

The spectra of velocity components are generalized within the framework of mixed-layer similarity. The characteristic wavelength for w increases linearly with height up to $z=0.1z_i$ following free convection prediction, but approaches a limiting value of $1.5z_i$ in the upper half of the boundary layer. The characteristic wavelengths for u and v are maintained at approximately $1.5z_i$ down to heights very close to the ground. This limiting wavelength corresponds to the length scale of large convective elements which extend to the top of the boundary layer.

The behavior of the temperature specra above $0.1z_i$ cannot be generalized in the same manner. Below that height the θ spectra follow behavior observed in the surface layer; $z=0.1z_i$ is also the upper limit for the free convection predictions of the w and θ variances.

The high-order moments and the structure parameters reveal the strong influence of entrainment at heights above $0.5z_i$.

1. Introduction

An experiment to investigate the structure of turbulence in the atmospheric boundary layer was conducted in 1973 by members of the Air Force Cambridge Research Laboratories (AFCRL), Bedford, Mass., the Meteorological Research Unit (MRU), Cardington, Bedford, England, and the Air Weather Service, Tinker Air Force Base, Okla. The experiment was carried out over a flat, sparsely populated section of northwestern Minnesota, 80 km south of the Canadian border.

This joint experiment was the culmination of nearly four years of preparation following the 1968 Kansas surface layer experiment (Haugen *et al.*, 1971). The Kansas experiment provided a comprehensive picture of turbulence structure in the surface layer, but it also indicated a clear need for similar data from greater heights. Turbulence in the surface layer appeared to be strongly influenced by scales of motion large enough to encompass the whole boundary layer. By the late 1960's scientists at MRU had developed turbulence probes which could be attached to the tethering cable of large, captive balloons (Readings and Butler, 1972) and had gained considerable experience gathering data to heights of the order of 1 km. It appeared that such a technique could easily be integrated with the instrumentation and data handling capability developed at AFCRL for tower-based measurements.

Before any full-scale experiment could be mounted it was necessary to establish that the two techniques were compatible. Experiments were conducted to determine whether differences in sensor design, frequency response, data reduction techniques and the movement of the MRU probe as it swayed with the balloon cable produced significant differences in the observations. The first comparison test, performed at Bedford, Mass., in 1969, showed excellent agreement in the means, variances and covariances of velocity components and temperature when the two sensors were mounted 2 m apart on a 16 m tower (Readings

[1] Present affiliation: Wave Propagation Laboratory, NOAA, Boulder, Colo. 80302.

[2] Present affiliation: Wave Propagation Laboratory, NOAA, Boulder, Colo. 80302 and Cooperative Institute for Research in Envrionmental Sciences, University of Colorado/NOAA, Boulder, Colo. 80309

[3] Present affiliation: Ministry of Defense, Whitehall, London, England.

and Butler, 1972). The second test, designed to isolate possible effects of cable movement on the measured statistics, was conducted in 1971 on a 370 m tower (Haugen *et al.*, 1975) at Eglin AFB, Fla. The AFCRL sonic anemometers were mounted on booms at 150 and 305 m, while the MRU probes were flown at the same heights on the tethering cable of a 1300 m³ kite balloon. The results showed that the mean and variance of the horizontal wind speed were overestimated (about 10% and 20%, respectively) by the balloon-borne probe, but the variances of the vertical wind component and temperature and the fluxes of momentum and heat compared well. Spectrum analysis of these data provided essential information on the distribution of probe movement error needed to correct velocity spectra obtained subsequently at the Minnesota site.

2. Experimental details

The tower and balloon-launch facilities for the Minnesota experiment were located on the southern edge of a flat uniform 1 mi² plot of land. At the time of this experiment most crops in the area had been harvested, so the fetch in the northerly direction was uniform in its roughness for about 10 km. Only differences in color that normally exist between freshly harvested, plowed and fallow areas remained as inhomogeneities in terrain cover. A description of the site with plot plan and aerial photographs of installations at the site can be found in a paper by Readings *et al.* (1974).

AFCRL's profile and turbulence sensors were mounted on a 32 m tower. The tethered balloon launch and mooring point was 90 m east-southeast of the tower. Two-axis sonic anemometers were used for measuring mean horizontal winds at 1, 2, 4, 8, 16 and 32 m. Quartz-crystal thermometers measured mean temperatures at 0.5 m in addition to the heights listed above. Wind component and temperature fluctuations were measured with three-axis sonic anemometers and fine platinum-wire thermometers at 4 and 32 m on the tower. Five MRU probes were used for the balloon-borne measurements. These were the same probes used in the comparison experiments except for a modification to measure azimuth wind direction. The heights at which they were flown varied from one observational period to another, depending on operating conditions. The maximum height range was 61 to 1219 m.

During periods of data gathering, the actual heights of the probes were measured periodically with a double theodolite system. Their motions were also monitored by tracking a rawinsonde attached to the balloon cable just above the top probe. Slow-rise rawinsonde ascents made every 2 h during observational periods by the Mobile Weather Squadron, Air Weather Serivce, provided information on wind and temperature fields above the instrumented heights. From these data we were able to determine the height of the lowest inversion base, the upper limit of the convective boundary layer and its variation as a function of time.

Data collection was restricted to periods when the wind was northerly. The sky was clear during the periods chosen for this study, with occasional patches of cirrus clouds visible around the horizon. As it happened, each period began during convective conditions, usually late morning or early afternoon. An observational period was terminated when either wind speed or direction became unfavorable or when turbulence at all levels vanished as often happened around midnight. The northerly winds occurred with high pressure systems moving over the site rapidly. Thus the period of consistent northerly winds seldom lasted more than 12 h. As a result, the data obtained are effectively restricted to the convective boundary layer.

All data recording was accomplished by the AFCRL computer-controlled data acquisition system (Kaimal *et al.*, 1966). The turbulence probes on the tower and the balloon cable were sampled 10 times per second; the wind and temperature profile sensors on the tower, once a second. Details of the experimental techniques and the data reduction procedures are reported by Izumi and Caughey (1976). Eleven 75 min periods of observations of the convective boundary layer provide the data base for the analyses described in this paper.

3. Description of data

The observational periods included in this study are listed in Table 1. They all fall within the time interval 1200–1800 CDT, when the height of the inversion base was roughly constant and the surface heat flux was directed upward. Listed in Table 1 are time periods for each run, the average values of the height of the lowest inversion base, the surface heat flux and other relevant boundary layer parameters. The reference heights for the five MRU probes are given in Table 2. The common averaging period for all data is 75 min. The fluctuation data are filtered with a high-pass, recursive digital filter to minimize long-term trends. The filter effectively attenuates frequencies below 0.001 Hz (12 dB per octave roll-off with −3 dB point at 0.001 Hz). A detailed discussion of data-reduction procedures is given by Izumi and Caughey (1976).

Computation of spectra and cospectra followed procedures used earlier in the analysis of the Kansas data (Kaimal *et al.*, 1972). The available bandwidth was covered in overlapping stages: the higher range (0.0025–5.0 Hz) by dividing each 75 min segment into shorter segments and averaging the spectral estimates over frequency bands, the lower range (0.0002–0.04 Hz) by block-averaging the original time series to reduce the number of points. The low-frequency ends of the spectra were later corrected for the attenuation caused by the high-pass filter.

TABLE 1. List of runs with significant boundary-layer parameters expressed in MKS units.

Run	Date	Period (CDT)	Q_0	u_*	$-L$	z_i	w_*	θ_*
2A1	10 Sept 73	1217–1332	0.196	0.45	41.7	1250	2.00	0.098
2A2	10 Sept 73	1332–1447	0.209	0.45	38.0	1615	2.23	0.094
3A1	11 Sept 73	1510–1625	0.186	0.37	24.0	2310	2.41	0.077
3A2	11 Sept 73	1625–1714	0.116	0.32	24.3	2300	2.06	0.056
5A1	15 Sept 73	1622–1737	0.069	0.18	7.1	1085	1.35	0.051
6A1	17 Sept 73	1401–1516	0.210	0.24	5.7	2095	2.43	0.086
6A2	17 Sept 73	1516–1631	0.162	0.23	6.4	2035	2.21	0.073
6B1	17 Sept 73	1652–1807	0.072	0.26	22.7	2360	1.77	0.041
7C1	19 Sept 73	1415–1530	0.221	0.28	8.8	1020	1.95	0.114
7C2	19 Sept 73	1530–1645	0.181	0.30	13.1	1140	1.89	0.096
7D1	19 Sept 73	1650–1805	0.099	0.25	13.5	1225	1.58	0.063

4. General characteristics of the boundary layer

The convective boundary layer is defined as that part of the atmosphere most directly affected by solar heating on the earth's surface. In mid-latitudes over land, this layer typically reaches a height of 1–2 km by midafternoon. Its upper limit is often delineated by a capping inversion. This layer exhibits a near-constant distribution of wind speed and potential temperature, obviously a consequence of the strong vertical mixing produced by convection. The name "mixed layer" is therefore used synonymously with the convective boundary layer in much of the literature on the subject.

The wind speed and temperature profiles of Fig. 1 are fairly typical of daytime convective conditions. Almost all the wind shear and all the potential temperature gradient in the boundary layer are confined to a very shallow region close to the ground. The sharp increase in wind speed across the capping inversion appears consistently in many daytime runs and has possible implications for momentum and heat transport in the upper regions of the boundary layer. It should be pointed out that the dashed portion of the curves is obtained from rawinsonde measurements and tends to be less precise than those from the balloon-borne measurements. Also, the rawinsonde data are obtained from discrete observations made every 2 hr, while the solid curves represent a 75 min average. However, the strong winds observed above the inversion in successive rawinsonde ascents suggest a fairly persistent pattern of wind shear across the inversion in the early afternoon runs analyzed here.

TABLE 2. Reference heights (m) for the balloon-borne probes.

Run	Probe 1	Probe 2	Probe 3	Probe 4	Probe 5
2A1	61	305	610	914	1219
2A2	61	305	610	914	1219
3A1	61	152	305	457	610
3A2	61	152	305	457	610
5A1	61	152	305	457	610
6A1	152	305	610	914	1219
6A2	152	305	610	914	1219
6B1	152	305	610	914	1219
7C1	61	152	305	457	610
7C2	61	152	305	457	610
7D1	61	152	305	457	610

The boundary layer over land may be idealized as a three-layer structure in terms of the parameters considered relevant to the turbulence in each.[4] Proceeding upward from the surface, we have:

1) *The surface layer* where wind shear plays a dominant role. Here Monin-Obukhov similarity applies and the controlling parameters are z, τ_0, Q_0 and g/T. The scaling velocity and temperature for this layer are, respectively,

$$u_* = (\tau_0/\rho)^{\frac{1}{2}}, \tag{1a}$$

$$T_* = -Q_0/u_*. \tag{1b}$$

Dimensionless groups formed with u_* and T_* become universal functions of z/L. The Kansas results with the exception of u and v statistics support this (Businger *et al.*, 1971; Wyngaard and Coté, 1971; Kaimal *et al.*,

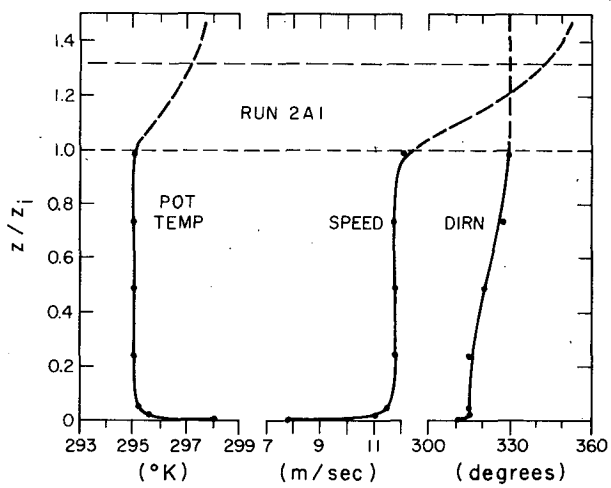

FIG. 1. Profiles of wind speed, wind direction and potential temperature for Run 2A1. The near-adiabatic lapse rate and the negligible mean wind shear in the mixed layer are typical for observational periods in this experiment.

[4] A list of symbols is given in an appendix.

1972; Busch, 1973). The shear layer is confined to a height range, $z<|L|$.

2) *The free convection layer* where τ_0 is no longer important but height z continues to be the significant length scale. The governing parameters reduce to three: z, Q_0 and g/T, which yield a scaling velocity u_f and a scaling temperature T_f given by

$$u_f=[Q_0 z(g/T)]^{\frac{1}{3}}, \tag{2a}$$

$$T_f=Q_0/u_f. \tag{2b}$$

Dimensionless groups formed with u_f and T_f should be constants according to the "local free-convection" predictions of Wyngaard *et al.* (1971a). The very unstable ($-z/L>1$) data from Kansas support these predictions for the most part. A definition of the upper limit for free convection scaling is one of the objectives of this analysis. Our data suggest an upper limit of approximately $0.1z_i$ for this layer.

3) *The mixed layer* where the structure of turbulence is insensitive to z as well as τ_0. The thickness of the boundary layer, defined as the height of the lowest inversion base z_i, emerges as the controlling length scale, so that the scaling velocity and temperature for this layer become

$$w_*=[Q_0 z_i(g/T)]^{\frac{1}{3}}, \tag{3a}$$

$$\theta_*=Q_0/w_*. \tag{3b}$$

Within this region dimensionless groups formed with w_* and θ_* should be functions only of z/z_i. This expectation is based on model studies (Deardorff, 1972; Wyngaard *et al.*, 1974) which show wind and temperature data scaling with w_* and θ_*. In the analyses to follow, the Minnesota data will be examined within the framework of such scaling.

Controversy exists regarding the choice of z_i for the thickness of the convective boundary layer. Some investigators (Tennekes, 1970; Zilitinkevich, 1972; Clarke and Hess, 1973) have suggested that this thickness is a function of u_*/f, the Ekman layer depth, but the modeling studies of Deardorff (1974a) show that z_i, the height of the lowest inversion base, determines the boundary layer depth. He found the heights of the boundary layer for both heat and momentum to be nearly the same and approximated by z_i.

Estimating z_i presented no difficulty in our observations as the base of the capping inversion was sharply defined in all the rawinsonde plots. The height of the inversion base varied from day to day and from one observational period to another, but its diurnal trend, at least in the limited sample obtained at Minnesota, followed a pattern which is typified by the curve in Fig. 2. Similar patterns have been observed with FM-CW radars (e.g., Richter *et al.*, 1974) and acoustic sounders (e.g., Neff, 1975) at other sites. Also shown on the same plot is the diurnal trend of Q_0 observed during the experiments.

The following observations can be made from Fig. 2. Between sunrise and local noon (1300 CDT) z_i grew rapidly in response to the steadily increasing surface heat flux. The growth of z_i slowed down between 1300 and 1600 CDT as Q_0 reached its maximum value. The growth rate of z_i for this period agrees with the numerical model prediction of Mahrt and Lenschow (1976) which assumes a constant Q_0 for the 3 h following local noon. But as Q_0 decreased through the late afternoon, z_i began to level off to a nearly constant value which it maintained even after Q_0 turned negative.

Examining data obtained during the evening transition, we find the dissolution of the convective boundary layer to be rather abrupt, especially when compared to its evolution in the morning. The heat flux over the entire layer turned negative within minutes, but surprisingly this trend propagated downward from the top with Q_0 the last to cross zero. The transition took place almost an hour before sunset. With surface temperatures dropping rapidly after sunset, an inversion layer often developed near the ground and continued to deepen through the evening. Remnants of the capping inversion were found to persist through the development of the nocturnal boundary layer and some-

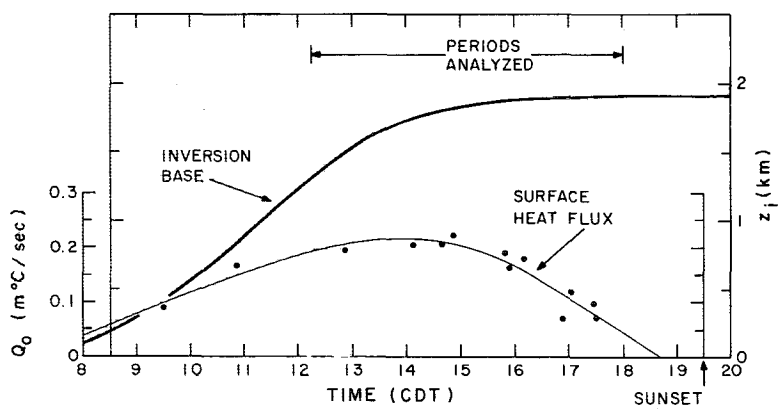

FIG. 2. Diurnal trend in the surface heat flux and corresponding inversion rise for a typical day.

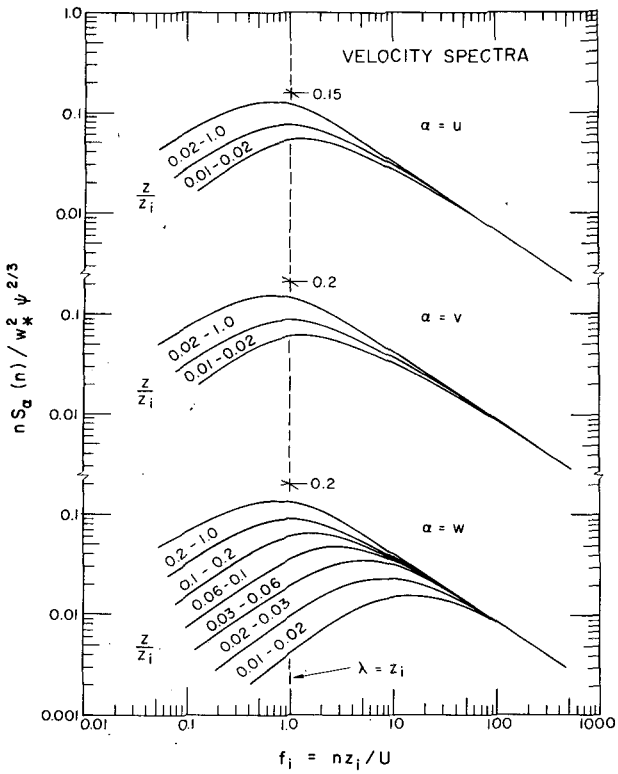

FIG. 3. Universal curves for velocity spectra expressed in mixed-layer similarity coordinates. The function ψ in the spectral normalization is the dimensionless energy dissipation rate $\epsilon/(g/T)Q_0$.

times well into the next morning, when they either merged with the newly rising surface inversion or existed as a separate layer aloft.

Even though the convective boundary layer evolves in response to the roughly sinusoidal variation in surface heating as described above, there is justification for treating its midday structure as if it were in steady state. The time scale characteristic of convectively driven turbulence is z_i/w_*. Under typical conditions ($z_i=1.25$ km, $Q_0=0.2$ m °C s^{-1}) this turns out to be 10 min, much smaller than the time scale of changes in Q_0 and z_i, or changes in the pressure field that drives the flow. Thus, we expect that near midday the mixed layer quickly adjusts its structure in response to the slowly changing boundary conditions and keeps itself in a condition of moving equilibrium or quasi-steady state. This quasi-steady state assumption is implicit in the analyses described in the sections to follow.

5. Spectra of velocity components

Data obtained in the 1968 Kansas experiment had shown that atmospheric spectra and cospectra from the first 22 m, when expressed in appropriate similarity coordinates, reduce to a set of universal curves that converge into a single curve in the inertial subrange, but spread out as a function of z/L at lower frequencies (Kaimal *et al.*, 1972). In this section we will attempt to see if the spectral properties of the convective boundary layer above 22 m can similarly be generalized through proper normalization of spectral intensities and frequency scales.

Two facts emerge as we examine velocity spectra obtained from the mixed layer. The energy in the inertial subrange remains essentially constant with height, in contrast with the sharp decrease with z observed near the ground, and the spectral peaks tend to be invariant both in their intensities and their positions on the frequency scale. These observations imply a near-uniform spectral behavior over much of the boundary layer, so the use of mixed-layer scaling appears logical. Extending the similarity argument to the mixed layer, we can expect the mixed-layer velocity spectrum, normalized by w_*^2, to be a function of only two variables, z/z_i and λ/z_i (where λ is the wavelength approximated by U/n). Thus, the one-dimensional logarithmic u spectrum in the inertial subrange can be expressed as

$$\frac{nS_u(n)}{w_*^2}=\frac{\alpha_1}{(2\pi)^{\frac{2}{3}}}\psi^{\frac{2}{3}}f_i^{-\frac{2}{3}}, \tag{4}$$

where α_1 is the spectral constant for u, ψ is the dimensionless dissipation rate ($\epsilon T/gQ_0$) appropriate to the mixed layer and f_i is the dimensionless frequency (nz_i/U) for that layer; ψ and f_i are analogous to ϕ_ϵ and f in the surface layer formulation [Eq. (5), Kaimal *et al.*, 1972]. By our similarity argument, ψ, the ratio of kinetic energy dissipation rate to buoyancy production rate at the surface, should be a function only of z/z_i.

Taking α_1 to be 0.5 and rearranging terms, Eq. (4) becomes

$$\frac{nS_u(n)}{w_*^2\psi^{\frac{2}{3}}}=0.15f_i^{-\frac{2}{3}}. \tag{5}$$

Spectral forms for the one-dimensional v and w spectra differ from Eq. (5) by a factor of $\frac{4}{3}$ as a consequence of isotropy, so that

$$\frac{nS_v(n)}{w_*^2\psi^{\frac{2}{3}}}=\frac{nS_w(n)}{w_*^2\psi^{\frac{2}{3}}}=0.20f_i^{-\frac{2}{3}}. \tag{6}$$

Logarithmic spectra normalized in this manner show systematic behavior when plotted as a function of f_i (see Fig. 3). Inclusion of $\psi^{\frac{2}{3}}$ in the normalization forces all spectra to collapse into a single curve in the inertial subrange. At lower frequencies we find the curves separating as a function of z/z_i. The separation is not nearly so systematic as in the Kansas spectra, but the demarcations between the different z/z_i categories in the composite plots are, nevertheless, clear enough to justify the curves in Fig. 3. Over 90% of the spectra in each z/z_i category fall within the areas indicated. The spectra used for constructing the composite plots

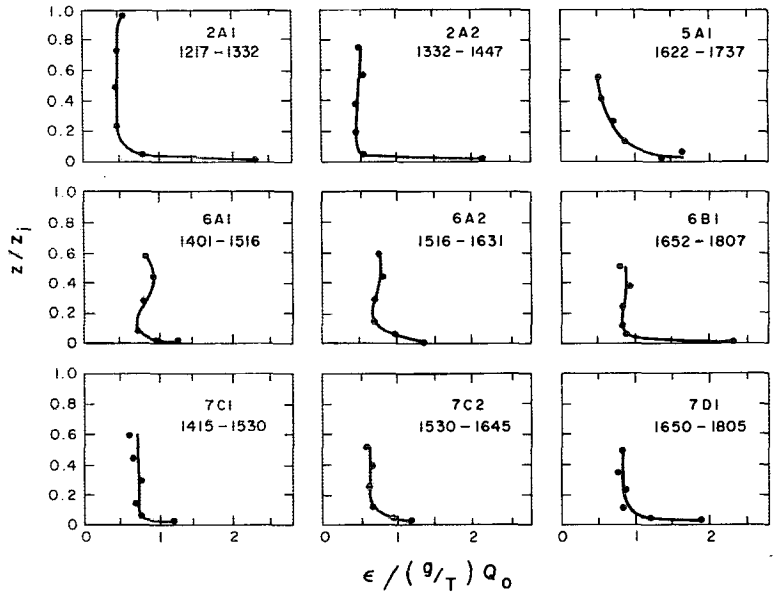

FIG. 4. Dimensionless energy dissipation rate ψ plotted as a function of z/z_i.

were subjected to minor smoothing by eye to average out the larger peaks and valleys near the low-frequency end. The only alterations made to the spectral shapes were the corrections for attenuation caused by the high-pass digital filter and the distortions introduced by balloon movement at the high-frequency end.

Of the three velocity components w shows the largest spread with height. Our normalization tends to exaggerate the spread in the ordinate, but the separation in the abscissa comes as no surprise because the length scales of w are known to be strongly height dependent in the lower layers of the atmsophere. As z/z_i increases from 0.01 to 1.0, the position of the spectral peak shifts to increasingly lower values of f_i rather rapidly at first up to $z/z_i=0.1$, then more gradually above that.[5] For u and v only two categories exist: 0.01 to 0.02 and 0.02 to 1.0, and the shift in spectral peak is virtually insignificant.

The dimensionless dissipation rate ψ, which appears in the normalization of the spectral intensities, assumes a nearly constant value in the mixed layer (see Fig. 4). In the fully convective runs this value falls between 0.5 and 0.7. Slightly larger values are observed in the near-transition runs close to sunset. In general these curves resemble the dissipation rate profiles obtained by Lenschow (1974), Frisch and Clifford (1974), Rayment (1973), Volkovitskaya and Ivanov (1970) and Kaimal and Haugen (1967). In the convective atmospheric boundary layer with negligible wind shear across the capping inversion, one would expect negligible shear-production rates of turbulent energy in the mixed layer. The height-averaged energy budget should then represent a balance between buoyant production and dissipation. With a linear heat-flux profile, one would then expect a mid-layer dissipation rate of 0.4–0.5 times the buoyant production rate. Our values are somewhat larger, perhaps because the large stress values observed at the Minnesota site caused appreciable shear production rates in some runs.

The limiting wavelength for the inertial subrange appears to be a function of z_i in the mixed layer. Based on Fig. 3 we can define the limit as $\lambda \leqslant 0.1z_i$. In the surface layer this limiting wavelength is approximately the height above ground (Kaimal *et al.*, 1972), so we have to assume the transition from the z to the z_i dependence occurs within the height range 0.01 to $0.1z_i$.

The peak wavelength λ_m in the w component also undergoes a similar transition with height. This wavelength is important for studies of turbulent transport in the boundary layer and therefore merits close examination. In Fig. 5 we have λ_m normalized with z_i, plotted as a function of z/z_i. At $z \leqslant 0.1z_i$ the relationship is a linear one approximated by

$$\lambda_m/z_i=5.9(z/z_i), \tag{7}$$

which is precisely the free-convection limit $z/\lambda_m=0.17$ observed in the Kansas data (Kaimal *et al.*, 1972). Above $0.1z_i$, λ_m increases more gradually with height and finally approaches a constant value ($\approx 1.5z_i$) in the range $0.5z_i<z<z_i$. An exponential relationship for its behavior above $0.1z_i$ has been suggested by D. H. Lenschow (personal communication) whose aircraft w spectra show similar behavior. Combining the results

[5] An alternate presentation of the spectra in free-convection layer scaling (i.e., normalizing with $u_f\psi^3$ and plotting against f) will cause all w spectra in the height range 0.01 to $0.1z_i$ to collapse into a single curve over the entire frequency range.

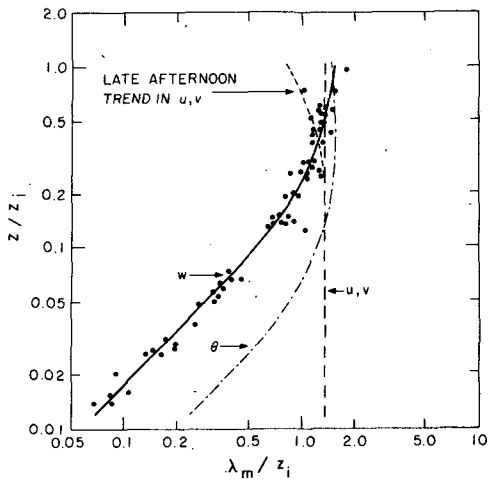

FIG. 5. Dimensionless peak wavelength for the velocity components and temperature plotted as a function of z/z_i. Scatter in the u, v and θ data points (not shown) is about twice as large as for w.

from Kansas[6] and Minnesota we can approximate λ_m for w in different regions of the convective boundary layer as follows:

$$(\lambda_m)_w \approx \begin{cases} z/(0.55-0.38|z/L|), & 0 \leqslant z \leqslant |L| \\ 5.9z, & |L| \leqslant z \leqslant 0.1z_i \\ 1.5z_i[1-\exp(-5z/z_i)], & 0.1z_i \leqslant z \leqslant z_i \end{cases} \quad (8)$$

For the u and v components λ_m/z_i shows little, if any, variation with z/z_i. The scatter in the data (not shown in this plot) is larger than for w, by at least a factor of 2. But their average value (1.3), shown by the dashed line, comes close to the asymptotic limit of 1.5 for w. Thus, in the mixed layer we see a strong tendency for the wavelength in all components to be the same and roughly equal to 1.5 times the boundary layer thickness.

A curious behavior observed toward the end of the day is noted in Fig. 5. In the runs immediately before sunset we see a contraction in the λ_m for u and v at the upper levels. No corresponding decrease is observed in w at the same heights.

These observations are in general agreement with those reported by other investigators. Deardorff's (1974b) numerical experiments showed λ_m/z_i for the w spectra to be approximately 1.0 for z/z_i between 0.38 and 0.69. The aircraft measurements of Kukharets (1974) showed λ_m for w increasing with height between 50 and 500 m and approaching a constant value above 500 m. He found λ_m sensitive to changes in terrain type (steppe, desert and ocean), which might possibly be the response to changes in z_i. The u spectra from the 300 m tower at Obninsk, reported by Ivanov *et al.* (1973), show behavior very similar to the Minnesota spectra. The single characteristic time scale observed at all levels on their tower is attributed to organized mesoscale convective circulations in the boundary layer.[7] In the surface layer we had found (Kaimal *et al.*, 1972; Busch, 1973) that λ_m for u and v do not obey Monin-Obukhov similarity under unstable conditions. The absence of any systematic behavior with z/L indicated that some length scale other than z and L controls the behavior of λ_m. It appears from our Minnesota data that this controlling length scale is z_i.

The low-frequency roll-off observed in our velocity spectra at $f_i<1.5$ (Fig. 3) appears to be real. It represents the limit of three-dimensional turbulence in the boundary layer. With the flow at synoptic scales being quasi-horizontal, the roll-off in w should continue to very low frequencies. The u and v spectra, on the other hand, should curve upward following the -3 power law (-2 slope in the logarithmic spectral representation) predicted for two-dimensional flows. The Wangara u spectra (Hess and Clarke, 1973) show a slope somewhat smaller, but nevertheless provide a fairly realistic representation of spectral behavior at very low frequencies. The existence of a spectral gap between the three-dimensional boundary layer turbulence and the quasi-horizontal large-scale motions, found in many recent observational studies (Hess and Clarke, 1973; Smedman-Högström and Högström, 1975) and strongly indicated by the low-frequency roll-off in our u and v spectra, appears to be a function of the spectral behavior in the mesoscale region. Energy contribution from large disturbances, like thunderstorms and frontal passages, would easily fill the gap, but the boundary layer as defined in this study would not exist during such periods. If the predominant scales of motion in the convective boundary layer are indeed controlled by the inversion height as implied in the Minnesota data, these scales will appear prominently in any spectral representation of the undisturbed boundary layer, and the gap separating this region from the synoptic scales of motion becomes an essential feature of boundary layer spectra.

This is a good point at which to speculate on the significance of the spectral peak at $\lambda_m \approx 1.5z_i$ observed in all three velocity spectra. Longitudinal roll vortices found in convective boundary layers with mean mixed-layer wind speeds in excess of 7 m s^{-1} (LeMone, 1973) come to mind, since they provide an effective mechanism for transporting heat and momentum between the earth's surface and the inversion base. The mean mixed-layer wind speeds for all runs used in this study (except Run 5A) exceed 7 m s^{-1}. LeMone (1973) has shown that these rolls have wavelengths roughly three times the boundary layer thickness. However, it is very unlikely that the rolls will appear in the logarithmic spectra at $\lambda_m \approx 1.5z_i$ because of their slow translation velocities across a fixed observation

[6] The 4 m Minnesota spectra are in exact agreement with the Kansas spectra and follow the relationship in Eq. (8) for $z<-L$.

[7] The small shift in the u and v spectral peaks at $0.01z_i<z<0.02z_i$ in Fig. 3 is more a reflection of the decreased U near the ground than an increase in n_m.

point. The rolls tend to line up at a small angle to the mean wind and move laterally at a fraction of the mean wind speed. The time interval between the passage of successive convergent zones shows up in the time traces of uw as periods of intense activity (Haugen *et al.*, 1971, and Section 7 of this paper) but it is seldom apparent in the velocity traces *per se*.

Interestingly enough, the observed λ_m matches the horizontal length scale of large convective plumes or thermals which extend through the depth of the boundary layer. The existence of organized convection on this scale has been observed by other investigators: Hardy and Ottersten (1969) and Konrad (1970) with the help of high-powered radars, Rowland and Arnold (1975) with FM-CW radar, and Frisch *et al.* (1975) with a combination of dual-Doppler radar, acoustic sounder and microbarograph array. In the Minnesota data evidence of such structures can be found in the temperature records from heights above $0.1z_i$ (see Section 7 for details). The temperature traces show positive bursts spaced 4–5 min apart, the time scale represented by λ_m in the mixed layer. The records show a high degree of correlation between these fluctuations and the long-period fluctuations in the velocity field responsible for the peaks in Fig. 3 which suggests that the length scales of three-dimensional turbulence in the boundary layer are determined primarily by the prevailing convection pattern. In the u and v components, where the length scales are not limited by the height above ground as in w, those long-period fluctuations can be observed down to very small heights above the ground.

The prevailing convective field during these runs probably resembles the "thermal streets" in Konrad's (1970) radar observations, where individual thermals line up in the direction of the mixed-layer mean wind vector (spaced roughly $1.5z_i$ apart and transported at the mean wind speed) with a row separation approximating $3z_i$, the roll wavelength observed by LeMone (1973). Under more unstable conditions (mean mixed-layer wind speeds <7 m s^{-1}), the pattern could conceivably be different, with individual thermals arranging themselves into open rings or hexagons with diameters 5-6 times z_i as observed by Hardy and Ottersten (1969). Such a pattern could yield the longer wavelengths ($6z_i$) observed by Fitzjarrald (1976) under low wind conditions. More observations and analysis of convection patterns are needed to confirm these speculations.

6. Spectrum of temperature

The spectrum of temperature, unlike velocity spectra, cannot be conveniently generalized within the framework of mixed-layer similarity. The difficulty stems mainly from run-to-run variations in the low-frequency variance introduced by entrainment effects in the upper half of the boundary layer. However, some broad generalizations can be made about spectral shapes and

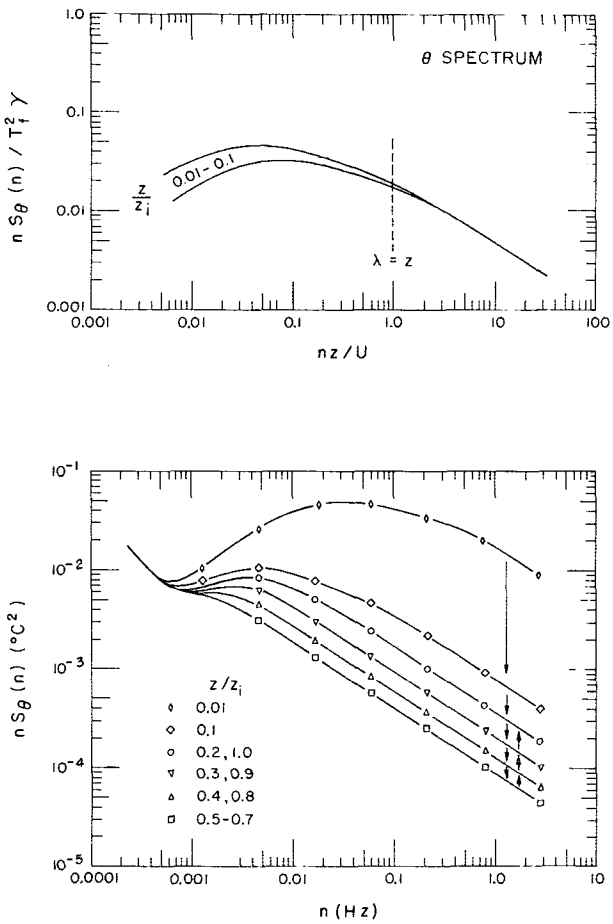

FIG. 6. Universal curve for the θ spectrum (upper figure) in the range $0.01z_i \lesssim z \lesssim 0.1z_i$. T_f is the free-convection scaling temperature and γ represents a dimensionless grouping which is constant (≈ 0.83) in this height range. Idealized temperature spectra in dimensional coordinates (lower figure) show variation in spectral behavior as a function of z/z_i.

inertial subrange intensities in the convective boundary layer. These generalizations are embodied in the set of idealized spectral curves shown in the lower plot of Fig. 6. At the low-frequency end they all converge to a single curve which extends upward in response to the diurnal trend in temperature. At inertial subrange frequencies the spectral intensity drops steadily with height up to $0.5z_i$, stays at a low value between 0.5 and $0.7z_i$ and starts to rise again above $0.7z_i$. The arrows near the right edge of the figure illustrate this trend. The leveling off and subsequent increase in the spectral level in the upper regions of the boundary layer clearly reflect the mixing produced by the entrainment of warm air through the capping inversion. Further evidence of this entrainment will be presented in Section 7.

The only region where spectral generalization is possible is in the height range $z \lesssim 0.1z_i$, where the θ spectra behave much like those obtained in the Kansas experiment (Kaimal *et al.*, 1972). Since the controlling

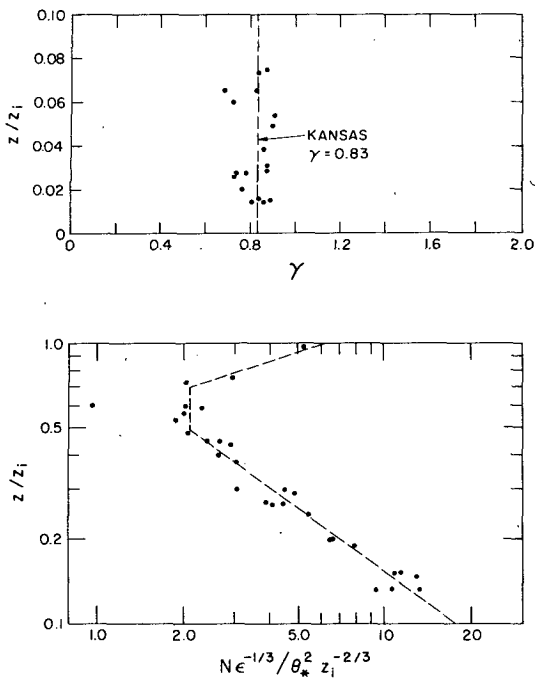

FIG. 7. The upper figure shows γ plotted as a function of z/z_i. The dashed line corresponds to the value 0.83 obtained in the Kansas experiments. In the lower figure the behavior of $N\epsilon^{-\frac{1}{3}}$ with height is presented in mixed-layer coordinates.

length scale in this region is z, not z_i we use f for the dimensionless frequency scale.

The logarithmic one-dimensional θ spectrum for the inertial subrange can be expressed in the form (Kaimal *et al.*, 1972)

$$nS_\theta(n)=\frac{\beta_1}{(2\pi)^{\frac{2}{3}}}N\epsilon^{-\frac{1}{3}}z^{\frac{2}{3}}f^{-\frac{2}{3}}, \tag{9}$$

where β_1 is the spectral constant for θ assumed to be 0.8 from the Kansas results, and N is the dissipation rate of $\theta^2/2$. Substituting the value for β_1, normalizing the spectral intensity with T_f^2, where T_f is the free-convection scaling temperature and rearranging terms, we have

$$\frac{nS_\theta(n)}{T_f^2\gamma}=0.235f^{-\frac{2}{3}}, \tag{10}$$

where

$$\gamma=N\epsilon^{-\frac{1}{2}}Q_0^{-\frac{1}{2}}(g/T)^{\frac{1}{2}}z^{\frac{1}{2}}. \tag{11}$$

This normalization brings all θ spectra into coincidence in the inertial subrange as seen in Fig. 6. At mid and low frequencies they collapse into a relatively narrow band with no apparent tendency to separate according to z/z_i. λ_m for this composite spectrum approximates $20z$, the free-convection limit in the Kansas spectra (Kaimal *et al.*, 1972). As z approaches $0.1z_i$ we see λ_m approaching the characteristic wavelength $1.5z_i$ found in the velocity components (see Fig. 5). Above $0.1z_i$, λ_m shows a tendency to increase slightly with height up to $0.5z_i$ and to decrease again above $0.7z_i$ consistent with the idealized spectral behavior in Fig. 6.

The function γ is essentially a dimensionless form of the structure parameter C_T^2. We can write

$$C_T^2=4\beta_1N\epsilon^{-\frac{1}{3}}\approx 3.2N\epsilon^{-\frac{1}{3}}. \tag{12}$$

The Kansas data provide the relationship between C_T^2 and surface layer parameters for local free convection (Wyngaard *et al.*, 1971b):

$$C_T^2\approx 2.67Q_0^{\frac{4}{3}}(g/T)^{-\frac{2}{3}}z^{-\frac{4}{3}}. \tag{13}$$

From Eqs. (11), (12) and (13), we have $\gamma\approx 0.83$ for the free-convection layer. The plot in Fig. 7 shows this approximation is valid for the Minnesota data as well. The value of γ stays surprisingly constant up to $0.5z_i$, indicating that the $z^{-\frac{4}{3}}$ decrease in the inertial subrange intensity continues well above $0.1z_i$. The behavior of $N\epsilon^{-\frac{1}{3}}$ above $0.1z_i$, nondimensionalized with mixed layer parameters θ_* and z_i, is shown in Fig. 7 and can be approximated as

$$\frac{N\epsilon^{-\frac{1}{3}}}{\theta_*^2z_i^{-\frac{2}{3}}}=\begin{cases}0.83(z/z_i)^{-\frac{4}{3}}, & z\leqslant 0.5z_i\\ 2.1, & 0.5z_i\leqslant z\leqslant 0.7z_i\\ 6.1(z/z_i)^3, & 0.7z_i\leqslant z\leqslant z_i\end{cases} \tag{14}$$

This behavior of the temperature spectrum agrees qualitatively with the ϵ and N profiles presented by Caughey and Rayment (1974).

The above empirical relationship can be used to collapse all inertial-subrange temperature spectra into a single curve in a plot similar to Fig. 3. Here the dimensionless ratio of Eq. (14) plays the same role as $\psi^{\frac{2}{3}}$ in Eq. (5). Bringing the inertial-subrange θ spectra together in this manner causes the low-frequency end to spread out, but no systematic trend emerges in the composite plots because of run-to-run variations in the details of their low-frequency behavior.

7. Heat flux and stress

The cospectra of heat flux and stress measured near the ground ($z<0.1z_i$) follow the same universal forms observed in the Kansas data (Kaimal *et al.*, 1972). But cospectral shapes depart significantly from those forms as z exceeds $0.1z_i$ and as large excursions in both positive and negative directions become a characteristic feature of heat flux and stress cospectra in the mixed layer. The patterns that emerge are not consistent enough to justify development of universal forms, although individually they provide interesting perspective into the nature of turbulent transport in the boundary layer.

In Fig. 8, for example, we see how the range of frequencies contributing to the upward transport of heat near the ground narrows down to a relatively small band centered around 0.003 Hz (the frequency corresponding to λ_m) at a height of 610 m. At 1219 m,

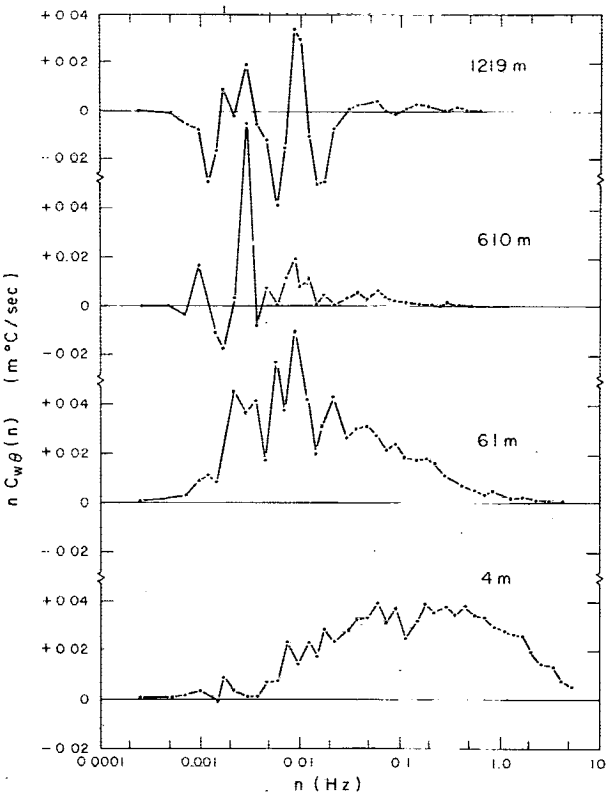

FIG. 8. Cospectra of heat flux at four heights during Run 2A1.

close to the inversion base, there is still some upward flux at 0.003 Hz, but the net flux is distinctly downward. Adiabatic transport of air downward through the capping inversion would produce this negative flux which, in turn, suggests substantial entrainment of air into the boundary layer from above (Ball, 1960). The temperature and heat flux traces in Fig. 9 provide clear evidence of such entrainment. Only portions of the $w\theta$ traces where significant heat flux exists are shown and these regions are shaded to distinguish them from the temperature traces. The regions of upward heat flux are obviously thermals which originate near the surface shear layer. The regions of downward heat flux appear between the tops of the thermals, but these are also characterized by positive bursts in the temperature trace. The structure of the bursts strongly suggest that the entraining warm air descends in the form of discrete plumes. They display a characteristic saw-tooth appearance with the largest discontinuity and the highest temperatures at the leading edge, not at the trailing edge as in buoyant plumes near the earth's surface (Kaimal and Businger, 1970). Such a structure is not surprising because the warmer air from higher up in the inversion layer has proportionally higher wind speeds (assuming positive wind shear across the inversion) and will therefore tend to concentrate on the downwind side of the plume.

The shape of the updraft region in the thermals, as delineated by the curves in Fig. 9, resembles the three-

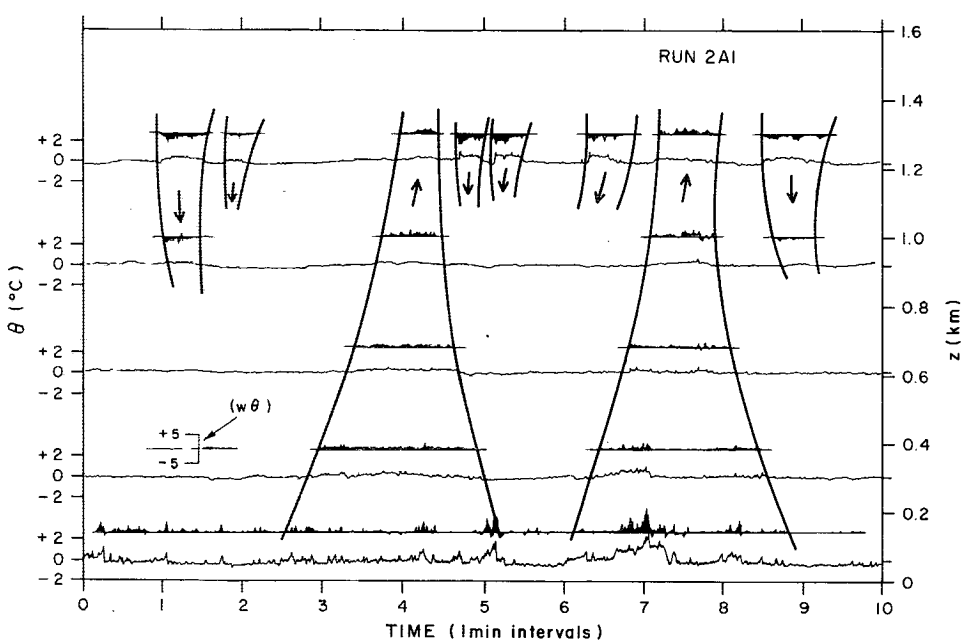

FIG. 9. Temperature fluctuations observed during the 10 min period from 1321 and 1331 CDT toward the end of Run 2A1. The top of the figure represents the inversion base for this period. The instantaneous vertical heat flux at each level is indicated by the shaded fluctuations traced above it. Only regions of significant flux are shown. Scale for $w\theta$ is in m °C s^{-1}.

dimensional convection patterns observed by Frisch *et al.* (1975) with their dual-Doppler radar. According to our observations these thermals develop from the merging of smaller ground-based plumes (Kaimal and Haugen, 1967; Kaimal and Businger, 1970) in the vicinity of $0.1z_i$ and extend to the top of the boundary layer. The observations of Arnold *et al.* (1975) and Rowland and Arnold (1975) suggest that this rising air spreads out laterally as it reaches the inversion base, producing a dome-like depression at the interface, and returns as a downdraft along the "sidewall" of the thermal. Arnold *et al.* find the dome-like structures, observed by their FM-CW radar, to be co-located with the thermals detected simultaneously in the lower boundary layer by their acoustic sounder. The juxtaposition of the cool moist air in the interior of the thermal with the warmer drier air above it makes the top dome visible to radars. But the strong returns from the sidewalls indicate the presence of entrained air from the inversion in the downdraft. The inverted *U* structures in the vertical sections and doughnut-shaped patterns in the plan views observed by Hardy and Ottersten (1969) and by Konrad (1970) thus represent the sidewalls where refractive index gradients are large enough to produce radar returns.

Arnold *et al.* conclude from their data that most of the entrainment takes place along the top of the dome. Here, either the Kelvin-Helmholtz instability described by Rayment and Readings (1974) or the wave-like overturning of the dome structure envisaged by Carson and Smith (1974) could provide the mechanism for entrainment. But the mechanism responsible for drawing this entrained air deep into the mixed layer, where its effects can be observed to heights of the order of $0.5z_i$, must be the downdraft in the gap between the thermals. The Doppler wind measurements of Hall *et al.* (1975), Rowland and Arnold (1975) and the Minnesota results described here seem to support this view. Laboratory convection experiments, now being conducted by G. E. Willis (personal communication) at the National Center for Atmospheric Research, simulating an inversion layer overlying the mixed layer, show tongues of fluid from the inversion being drawn into the mixed layer by the return flow between thermals. The separation distance for these thermals range from 1.3 to $1.4z_i$.

In our results, the consequences of entrainment are most apparent in the profiles of vertical heat flux (see Fig. 10). The negative heat flux below the inversion is quite apparent. Profiles observed around midday are generally similar to those from aircraft measurements (Lenschow, 1974; Pennell and LeMone, 1974), laboratory experiments (Willis and Deardorff, 1974) and model calculations (Deardorff, 1972; Wyngaard and Coté, 1974). They are approximately linear and cross zero somewhere in the upper half of the mixed layer. Zilitinkevich (1975) and Tennekes (1975) have recently discussed how the rate of growth of the convective layer can affect heat flux near z_i. Unfortunately, the uppermost instrument levels for most runs were well below z_i, so nothing very specific can be said about the magnitude of the negative heat flux in relationship to Q_0. But Fig. 10 demonstrates how variable the heat flux profile can be from one run to another and how the transition to negative flux is initiated near the top of

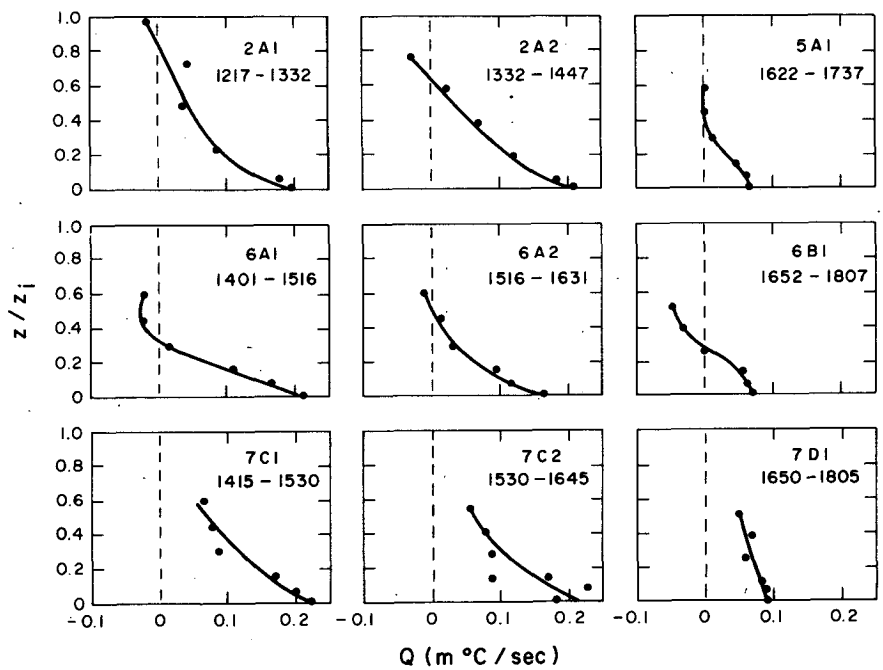

FIG. 10. Vertical profiles of heat flux for nine of the runs observed.

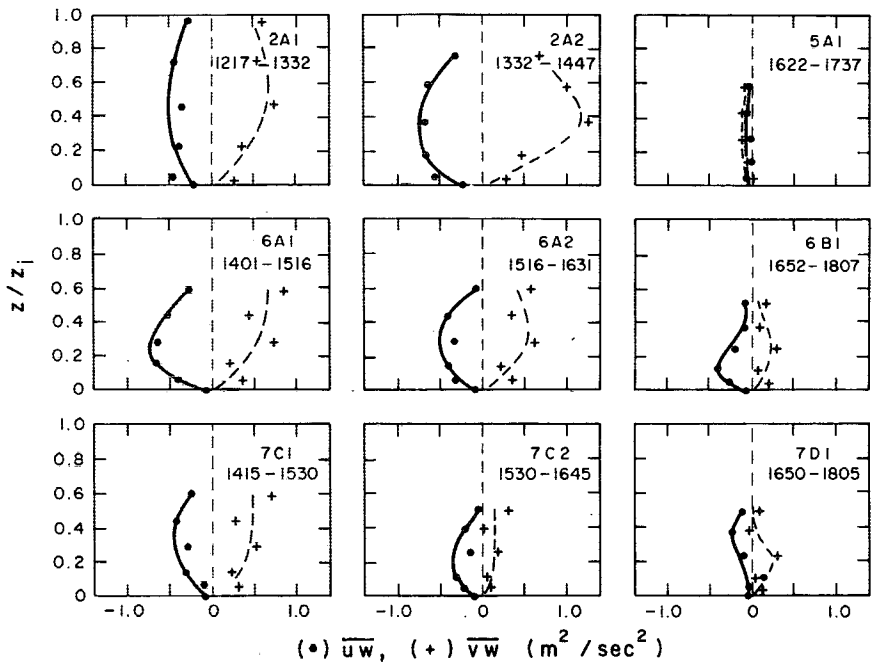

FIG. 11. Vertical profiles of stress for nine of the runs observed. The coordinate axes for u and v are referred to the mean wind field at the 4 m level.

the mixed layer even before the surface heat flux drops to zero at the end of the day.

The behavior of the stress profiles provides the largest surprise of all. Fig. 11 shows $\overline{uw}$ and $\overline{vw}$ increasing in magnitude with height, reaching a maximum value near $0.5z_i$ and decreasing above that height. In this figure the coordinate system for the stress components is referred to the vector-mean direction at 4 m. In the barotropic, nonentraining, convective boundary layer one would expect $\overline{uw}$ to decrease monotonically with height, approaching zero at $z=z_i$, and $\overline{vw}$ to vanish over the entire depth. The profiles in Fig. 11 look quite different: they are strongly curved, with $\overline{uw}$ and $\overline{vw}$ of approximately the same magnitude. Large stress values of this magnitude can arise from several causes. One possible cause may be baroclinicity (Arya and Wyngaard, 1975). The baroclinicity needed to explain these observations require positive horizontal temperature gradients of the order of 1°C per 15 km to the northwest, a condition not present on the synoptic scale during the experiments. Gradients of this magnitude are likely to be on the 1–2 km scale because of albedo variations introduced by differences between harvested and plowed areas. Whether such gradients existed on scales large enough (20–30 km) to affect the stresses is not known.

Deardorff (1973) has shown that a wind profile such as the one observed in Fig. 1 can generate large stresses through entrainment of momentum in the upper portions of the mixed layer. We tested this idea through a numerical simulation of Run 2A1 using the updated higher-order-closure model described by Wyngaard (1975). The observed values of surface geostropic wind, surface roughness and Q_0 for Run 2A1 were used. A barotropic model with no subsidence at z_i was assumed. Initial wind and temperature profiles at the morning transition were assumed and the model then calculated the evolution of the convective boundary layer. The calculated wind and stress profiles for the time corresponding to Run 2A1 are shown in Fig. 12. The results compare well with observations, except for the fact that the stress maxima occur in the vicinity of the inversion and not well within the boundary layer.

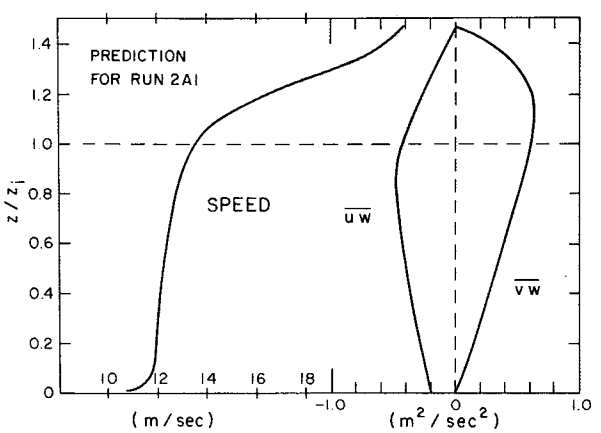

FIG. 12. Numerical predictions for wind speed and stress profiles for Run 2A1. Actual observations are given in Figs. 1 and 11.

Another possible explanation for the large stresses is that our averaging period is too short to include the entire range of cospectral contributions to the stress. Given a sufficiently long averaging period (or measurements over sufficiently long distances with an instrumented aircraft), the stress profile might possibly show a steady decrease with height. Implicit in the argument is the assumption that cospectral contributions from frequencies outside the present spectral bandwidth will be sufficient to offset the large contribution now measured in the range $0.001<n<5$ Hz. In the case of *uw* this would mean a large upward transport of momentum at very low frequencies ($n<0.001$ Hz). This argument cannot be discounted without definite proof to the contrary. A few runs (6A1 and 6A2) show evidence of positive *uw* and negative *vw* correlations at the low end of the cospectrum, but how far that trend continues beyond our spectral bandwidth cannot be ascertained. It is conceivable that the large stresses we observe result from a combination of factors, not any one by itself, so that even a small loss of cospectral energy at the low-frequency end could be significant. More data over longer averaging periods are needed to determine the relative importance of the various factors discussed here.

However, data obtained in this experiment provide some interesting details of the momentum transport process. The largest contributions to the stress cospectra come from frequencies in the range $0.002<n<0.1$ Hz, the energy-containing region for the velocity spectra. This range is at least a decade too low for balloon-movement effects (Haugen *et al.*, 1975) and other mechanically induced correlations. Fig. 13 shows *uw* traces for the 2.5 h period covering Runs 6A1 and 6A2 with the isopleths of 15 min averaged wind inclination angles observed by the MRU probes superimposed on them. The isopleths indicate well-defined longitudinal roll vortices with the updraft regions spaced roughly 1 h apart. Most of the vertical momentum transport in the boundary layer occurs within this updraft region. (Evidence of such roll circulation can be found in all the early afternoon runs selected for this study.) Within this updraft region the amplitude of the *uw* burst increases with height. This increase continues to a height of approximately $0.5z_i$. The downdraft region, on the other hand, is more diffused and occupies a longer time interval compared to the updraft region. Here the amplitude of *uw* fluctuations decreases rapidly with height and remains small throughout most of the boundary layer depth. The opposing stress gradients in the updraft and downdraft regions tend to cancel out in the surface layer, resulting in a near-constant distribution of stress with height; but above the surface layer in the time scale of our observations, the averaged stress profiles reflect the gradient in the updraft region.

Examining the structure of the *uw* bursts in the updraft region, we find that it consists of smaller discrete bursts with vertical continuity through the depth of the boundary layer. These small bursts in fact correspond to the thermals discussed earlier in this section. It appears that the bulk of the downward momentum transport in the boundary layer is carried out by the thermals located in the updraft regions between the longitudinal roll vortices. The convective elements in the downdraft region do not seem to play an active role in transporting momentum.

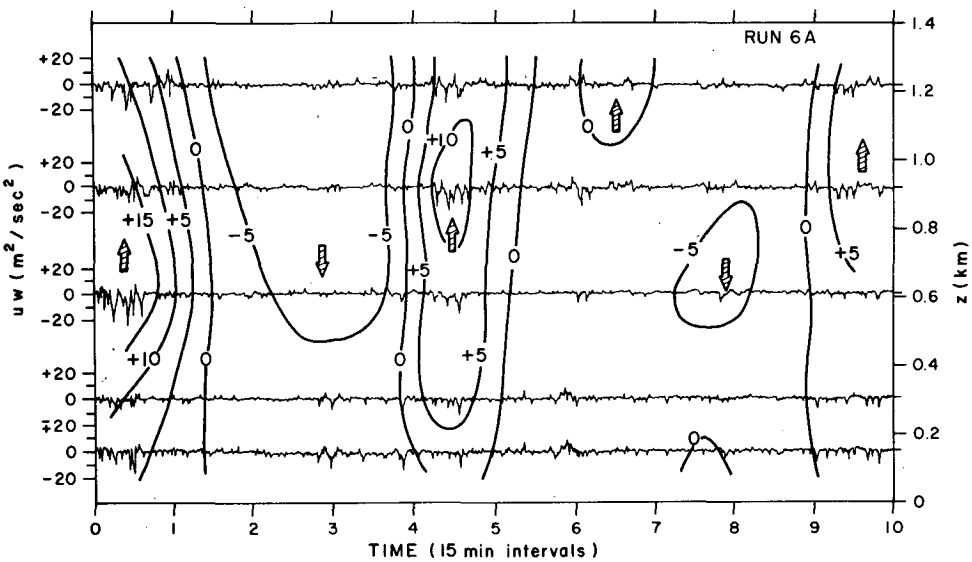

FIG. 13. Instantaneous *uw* at five levels observed during the 150 min period covering Runs 6A1 and 6A2. Isopleths of wind inclination angle (15 min averaged) at 5° intervals are shown superimposed on the *uw* fluctuations. Each division on the scale represents 15 min.

8. Moments and structure parameters

In this section we will examine the vertical profiles of some higher order moments and structure parameters to determine to what heights the Kansas free-convection predictions apply and how the profiles are modified by entrainment in the upper regions of the mixed layer. We had observed earlier that the free-convection predictions for the peak wavelengths in the w and θ spectra are valid to a height of $0.1z_i$. Above that they tend to stay approximately constant with height. Only the moments involving w and θ will be examined here because they are least affected by balloon-movement effects.

The asymptotic predictions for $\overline{w^2}$ and $\overline{\theta^2}$ expressed in terms of surface layer parameters (Wyngaard *et al.*, 1971a) are

$$\overline{w^2}/u_*^2 \approx 3.6(-z/L)^{\frac{2}{3}}, \tag{15}$$

$$\overline{\theta^2}/T_*^2 \approx 0.9(-z/L)^{-\frac{2}{3}}. \tag{16}$$

These expressions convert directly to mixed layer parameters with only a change in the value of the constant. Thus, replacing Eqs. (15) and (16) we have

$$\overline{w^2}/w_*^2 \approx 1.8(z/z_i)^{\frac{2}{3}}, \tag{17}$$

$$\overline{\theta^2}/\theta_*^2 \approx 1.8(z/z_i)^{-\frac{2}{3}}. \tag{18}$$

These predictions are shown as dashed lines in Fig. 14. We find the above predictions followed to a height of

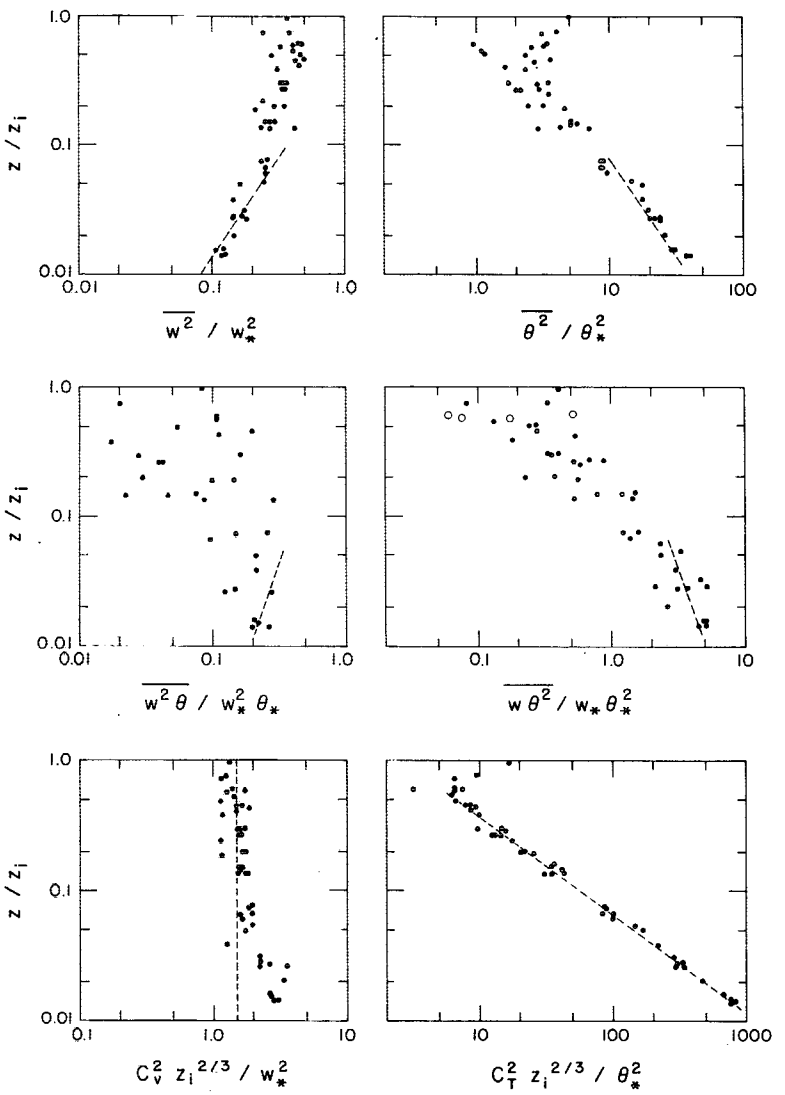

FIG. 14. Vertical profiles of high-order moments and structure functions for the fully convective runs in Table 1 (Runs 5A1, 6A1 and 7D1 are excluded). The dashed lines are free-convection predictions based on the Kansas data. The open circles represent negative values.

$0.1z_i$. (Only the fully convective runs are used in constructing these and other plots in Fig. 14.) Above $0.1z_i$ we see data points deviating from the predictions, exhibiting much more scatter than is apparent at the lower levels.

Comparing our w variance data above $0.1z_i$ with aircraft, water tank and numerical model results [as surveyed by Deardorff and Willis (1974)] we find the aircraft results fall within the scatter of our data points. The magnitudes observed in the tank and numerical experiments tend to be slightly larger than the atmospheric measurements. As for the height of maximum variance, the tank data show a peak around $0.5z_i$—as in the aircraft data and barely suggested in the Minnesota data—while the numerical model has its peak somewhat lower. The most significant departure from the tank and numerical results is the absence of any significant drop in w variance near the inversion base. This is consistent with the spectral behavior observed in Fig. 3 showing no appreciable change in spectral intensity or shape above $0.1z_i$ and probably reflects the different upper boundary conditions that exist in the atmosphere compared to the experiments.

The θ variance above $0.1z_i$ shows a steeper decrease with height than predicted by local free-convection similarity. The decrease continues to $0.5z_i$ where it reaches a minimum value. Above $0.5z_i$ the variance increases with height, clearly the result of mixing produced by entrainment of warm air into the boundary layer through the inversion.

The third-order moments $\overline{w^2\theta}$ and $\overline{w\theta^2}$, which represent the vertical transports of heat flux and temperature variance, respectively, deviate from their free-convection predictions at heights considerably below $0.1z_i$. The asymptotic values for these moments (Wyngaard *et al.*, 1971a) expressed in mixed-layer similarity parameters become

$$\overline{w^2\theta}/w_*^2\theta_* \approx 0.9(z/z_i)^{\frac{1}{3}}, \tag{19}$$

$$\overline{w\theta^2}/w_*\theta_*^2 \approx 1.1(z/z_i)^{-\frac{1}{3}}. \tag{20}$$

The vertical gradients of these triple moments represent the local gain or loss of the quantity ($\overline{w\theta}$ and $\overline{\theta^2}$, respectively) that results from turbulent transport. Eqs. (19) and (20) imply a local loss of $\overline{w\theta}$ and a local gain of $\overline{\theta^2}$ resulting from turbulent transport in their budget equations. Our observations show free-convection predictions approached at fairly low heights (0.02 and $0.05z_i$, respectively) for $\overline{w^2\theta}$ and $\overline{w\theta^2}$. In the case of $\overline{w^2\theta}$ even the sign of the gradient is different above $0.02z_i$ indicating a gain rather than a loss from turbulent transport in the $\overline{w\theta}$ budget. The transport term in the $\overline{\theta^2}$ budget remains a gain throughout. Note the negative values of $\overline{w\theta^2}$ (open circles) above $0.5z_i$ showing downward flux of temperature variance, another manifestation of the entrainment process discussed earlier.

The lack of agreement between the observations and predictions might very likely be a consequence of inadequate averaging time. With longer observational periods it is conceivable that the scatter in the results will be greatly reduced and the free-convection predictions will be followed to a height of $0.1z_i$ as in the second moments. On the other hand, it is possible that the turbulent transports of $\overline{w\theta}$ and $\overline{\theta^2}$ are in fact confined to a shallow layer around $0.1z_i$ and the data reflect the true state of affairs in the atmospheric boundary layer. Further measurements are needed to establish the reasons for the observed departures from prediction. Spatial measurements over long distances offer the best hope for statistically stable third moments, being free of contamination from the diurnal trends that inevitably affect single-point measurements.

The structure parameters C_V^2 and C_T^2 reflect the inertial subrange behavior in the velocity and temperature spectra, respectively. Their chief application is to studies of acoustic and optical propagation in the atmosphere. The expression for C_V^2, analogous to the one for C_T^2 in Eq. (12), is (Kaimal, 1973)

$$C_V^2 = 4\alpha_1\epsilon^{\frac{2}{3}} \approx 2\epsilon^{\frac{2}{3}}. \tag{21}$$

The asymptotic surface-layer prediction for C_V^2, derived from the surface layer relationship for ϕ_ϵ (Wyngaard and Coté, 1971), shows that

$$\frac{C_V^2 z_i^{\frac{2}{3}}}{w_*^2} = \text{constant}, \tag{22}$$

which is unity for the Kansas data but is higher (~ 1.5) for the Minnesota data. It is interesting that this constant value is reached only at heights above $0.1z_i$. A useful approximation for the dimensionless C_V^2 in the range $0.01z_i \leqslant z \leqslant 0.1z_i$ from Fig. 14 would be

$$\frac{C_V z_i^{\frac{2}{3}}}{w_*^2} = 1.3 + 0.1(z/z_i)^{-\frac{2}{3}}. \tag{23}$$

The C_T^2 measurements provide by far the best fit to the Kansas free-convection predictions in the lower half of the boundary layer with considerably less scatter than any other parameter examined. From Eqs. (12) and (14) we have

$$\frac{C_T^2 z_i^{\frac{2}{3}}}{\theta_*^2} = 2.67(z/z_i)^{-\frac{4}{3}}, \tag{24}$$

which is indicated by the dashed line in Fig. 14. These results are in agreement with Tsvang's (1969) observations that showed the $-\frac{4}{3}$ power law extending to heights of the order of 500 m in the atmosphere. The trend stops at about $0.5z_i$, and C_T^2 begins to increase with height above $0.7z_i$, once more reflecting the mixing

produced by warm air entraining into the boundary layer. This modification of the $-\frac{4}{3}$ law above $0.5z_i$ has also been observed by Neff (1975) from acoustic sounder returns over land and by Frisch and Ochs (1975) in aircraft measurements within the marine boundary layer.

9. Conclusions

The conclusions to emerge from this study can be summarized as follows:

1) The convective boundary layer observed at the Minnesota site was well-mixed down to approximately $0.1z_i$, with a near-uniform wind speed and potential temperature distribution over that depth. A well-defined capping inversion was observed in all daytime runs.

2) The spectra of velocity components in the boundary layer can be generalized within the framework of mixed layer similarity. With appropriate normalization the w spectrum can be reduced to a family of curves which spreads out as a function of z/z_i at low frequencies, but converge to a single universal curve in the inertial subrange. The u and v spectra generalized in the same manner show universal behavior, but without the z/z_i dependence apparent in w. The onset of the inertial subrange in the mixed layer occurs at wavelength $\lambda \approx 0.1z_i$.

3) The temperature spectra above $0.1z_i$ cannot be generalized in the same manner as the velocity spectra because of variability in the low-frequency behavior. However, the inertial subrange level is more predictable, decreasing as $(z/z_i)^{-\frac{1}{3}}$ up to $0.5z_i$ and increasing as $(z/z_i)^3$ above $0.7z_i$. Below $0.1z_i$ they behave much like the surface layer spectra.

4) The characteristic wavelength λ_m for w and θ increases linearly with z in the height range $-L$ to $0.1z_i$, following free-convection prediction, but levels off to a nearly constant value ($\lambda_m \approx 1.5z_i$) above that height. λ_m for u and v stays approximately the same (at $\lambda_m \approx 1.5z_i$) throughout the depth of the boundary layer.

5) The wavelength $\lambda_m \approx 1.5z_i$ observed in the velocity and temperature spectra corresponds to the length scale of large thermals that appear to dominate the circulation in the boundary layer.

6) Free-convection predictions for the variances of w and θ also appear valid to a height of $0.1z_i$. The triple moments indicate a much shallower free-convection layer but this may be the result of inadequate averaging time. C_V^2 reaches its asymptotic limit only above $0.1z_i$, while C_T^2 fits the prediction to a height of $0.5z_i$.

7) There is evidence of substantial heat and momentum entrainment into the boundary layer through the capping inversion. The entrained warm air descends in the form of inverted plumes strongly affecting the temperature and heat flux statistics in the upper half of the boundary layer. The unexpectedly large stress values observed in the boundary layer can be explained, at least partly, in terms of momentum entrainment across the velocity jump within the inversion. Any theoretical or numerical model for the mixed layer must take into account the effects of entrainment through its upper boundary.

Acknowledgments. The concept of the Minnesota experiment originated early in 1968 in discussions between Dr. Morton Barad and Dr. Frank Pasquill. The program would not have been possible without their continued support and encouragement.

The staff at MRU prepared and tested the balloon-borne instrumentation. Mr. Jim Newman and Mr. Robert Lynch (AFCRL) and Mr. Alan Marks (MRU) played vital roles in the operation and handling of the sensors and the data acquisition equipment in the field. Members of the Aerospace Instrumentation Laboratory (AFCRL) maintained and operated the kite balloon during the experiments. Mr. Larry Bass and Mrs. Jean O'Donnell (AFCRL) were responsible for computer processing of the data.

Finally, we are grateful to the Wave Propagation Laboratory (NOAA) for support provided in the preparation of the manuscript.

APPENDIX

List of Symbols

U	mean wind speed
u, v, w	fluctuating wind components in the longitudinal, lateral and vertical directions
T	mean temperature
θ	fluctuating temperature
ρ	density of air
τ_0	surface shear stress $[=-\rho\overline{uw}$ at 4 m$]$
Q	vertical kinematic heat flux $[=\overline{w\theta}]$
Q_0	surface kinematic heat flux $[=\overline{w\theta}$ at 4 m$]$
(g/T)	buoyancy parameter
ϵ	dissipation rate of turbulent kinetic energy
k	von Karman's constant
ϕ_ϵ	dimensionless dissipation rate $[=kz\epsilon/u_*^3]$
ψ	dimensionless dissipation rate $[=\epsilon T/gQ_0]$
N	dissipation rate for one-half of the temperature variance
γ	a dimensionless structure parameter
α_1	spectral constant for one-dimensional u spectrum
β_1	spectral constant for the one-dimensional θ spectrum
z	height above ground
z_i	height of lowest inversion base (from rawinsonde ascents)
L	Obukhov length $[=-u_*^3/k(g/T)Q_0]$
n	cyclic frequency

n_m frequency of logarithmic spectral peak
λ_m wavelength corresponding to $n_m[=U/n_m]$
f dimensionless frequency $[=nz/U]$
f_i dimensionless frequency $[=nz_i/U]$
$S(n)$ one-dimensional spectral density
C_T^2 structure parameter for temperature
C_V^2 structure parameter for velocity
u_*, T_* scaling velocity and temperature for the surface shear layer
u_f, T_f scaling velocity and temperature for the free-convection layer
w_*, θ_* scaling velocity and temperature for the mixed layer.

REFERENCES

Arnold, A., J. R. Rowland, T. G. Konrad, J. H. Richter, D. R. Jensen and V. R. Noonkester, 1975: Simultaneous observations of clear air convection by a pulse radar, an FM-CW radar, an acoustic sounder and an instrumented aircraft. *Preprints 16th Radar Meteorology Conf.*, 22–23 April, Houston, Tex., Amer. Meteor. Soc., 290–295.

Arya, S. P. S., and J. C. Wyngaard, 1975: Effect of baroclinicity on wind profiles and the geostrophic drag law for the convective planetary boundary layer. *J. Atmos. Sci.*, **32**, 767–778.

Ball, F. K., 1960: Control of inversion height by surface heating. *Quart. J. Roy. Meteor. Soc.*, **86**, 483–494.

Busch, N. E., 1973: The surface boundary layer. *Bound.-Layer Meteor.*, **4**, 213–240.

Businger, J. A., J. C. Wyngaard, Y. Izumi and E. F. Bradley, 1971: Flux-profile relationships in the atmospheric surface layer. *J. Atmos. Sci.*, **28**, 181–189.

Carson, D. J., and F. B. Smith, 1974: Thermodynamic model for the development of a convectively unstable boundary layer. *Advances in Geophysics*, Vol. 18A, Academic Press, 111–124.

Caughey, S. J., and R. Rayment, 1974: High-frequency temperature fluctuations in the atmospheric boundary layer. *Bound.-Layer Meteor.*, **5**, 489–503.

Clarke, R. H., and G. D. Hess, 1973: On the appropriate scaling for velocity and temperature in the planetary boundary layer. *J. Atmos. Sci.*, **30**, 1346–1353.

Deardorff, J. W., 1972: Numerical investigation of neutral and unstable planetary boundary layers. *J. Atmos. Sci.*, **29**, 91–115.

——, 1973: An explanation of anomalously large Reynolds stresses within the convective planetary boundary layer. *J. Atmos. Sci.*, **30**, 1070–1076.

——, 1974a: Three-dimensional numerical study of the height and mean structure of a heated planetary boundary layer. *Bound.-Layer Meteor.*, **7**, 81–106.

——, 1974b: Three-dimensional numerical study of turbulence in an entraining mixed layer. *Bound.-Layer Meteor.*, **7**, 199–226.

——, and G. E. Willis, 1974: Computer and laboratory modeling of the verical diffusion of nonbuoyant particles in the mixed layer. *Advances in Geophysics*, Vol. 18B, Academic Press, 187–200.

Fitzjarrald, D. E., 1976: A field observation of atmospheric free-convection. *J. Appl. Meteor.*, **15**, 259–263.

Frisch, A. S., and S. F. Clifford, 1974: A study of convection capped by a stable layer using Doppler radar and acoustic echo sounders. *J. Appl. Meteor.*, **31**, 1622–1628.

——, and G. R. Ochs, 1975: A note on the behavior of the temperature structure parameter in a convective layer capped by a marine inversion. *J. Appl. Meteor.*, **14**, 415–419.

——, R. B. Chadwick, W. R. Moninger and J. M. Young, 1975: Observation of boundary layer convection cells measured by dual-Doppler radar and echosounder and by microbarograph array. *Bound.-Layer Meteor.*, **3**, 199–226.

Hall, F. F., Jr., J. G. Edinger and W. D. Neff, 1975: Convective plumes in the planetary boundary layer. *J. Appl. Meteor.*, **14**, 513–523.

Hardy, K. R., and H. Ottersten, 1969: Radar investigation of convective patterns in the clear atmosphere, *J. Atmos. Sci.*, **26**, 666–672.

Haugen, D. A., J. C. Kaimal and E. F. Bradley, 1971: An experimental study of Reynolds stress and heat flux in the atmospheric surface layer. *Quart. J. Roy. Meteor. Soc.*, **97**, 168–180.

——, ——, C. J. Readings and R. Rayment, 1975: A comparison of balloon-borne and tower-mounted instrumentation for probing the atmospheric boundary layer. *J. Appl Meteor.*, **14**, 540–545.

Hess, G. D., and R. H. Clarke, 1973: Time spectra and cross-spectra of kinetic energy in the planetary boundary layer. *Quart. J. Roy. Meteor. Soc.*, **99**, 130–153.

Ivanov, V. N., A. Ye. Ordanovich and L. I. Petrova, 1973: Certain properties of wind-velocity and air-temperature spectra in the low-frequency range in the presence of convection. *Izv. Atmos. Ocean. Phys.*, **9**, 445–452.

Izumi, Y., and S. J. Caughey, 1976: Minnesota 1973 atmospheric boundary layer experiment data report. AFCRL Res. Rep. (in preparation). [Will be available on request from Y. Izumi, AFGL, Hanscom AFB, Bedford, Mass. 01731 or NTIS, Springfield, Va. 22151.]

Kaimal, J. C., 1973: Turbulence spectra, length scales and structure parameters in the stable surface layer. *Bound.-Layer Meteor.*, **4**, 289–309.

——, and D. A. Haugen, 1967: Characteristics of vertical velocity fluctuations observed on a 430 m tower. *Quart. J. Roy. Meteor. Soc.*, **93**, 305–317.

——, and J. A. Businger, 1970: Case studies of a convective plume and a dust devil. *J. Appl. Meteor.*, **9**, 612–620.

——, D. A. Haugen and J. T. Newman, 1966: A computer-controlled mobile micrometeorological observation system. *J. Appl. Meteor.*, **5**, 411–421.

——, J. C. Wyngaard, Y. Izumi and O. R. Coté, 1972: Spectral characteristics of surface layer turbulence. *Quart. J. Roy. Meteor. Soc.*, **98**, 563–589.

Konrad, T. G., 1970: The dynamics of the convective process in clear air as seen by radar. *J. Atmos. Sci.*, **27**, 1138–1147.

Kukharets, V. P., 1974: Spectra of the vertical wind velocity component in the atmospheric boundary layer. *Izv. Atmos. Ocean. Phys.* **10**, 375–378.

LeMone, M. A., 1973: The structure and dynamics of horizontal roll vortices in the planetary boundary layer. *J. Atmos. Sci.*, **30**, 1077–1091.

Lenschow, D. H., 1974: Model of the height variation of the turbulence kinetic energy budget in the unstable planetary boundary layer. *J. Atmos. Sci.*, **31**, 465–474.

Mahrt, L., and D. H. Lenschow, 1976: Growth dynamics of the convectively mixed layer. *J. Atmos. Sci.*, **33**, 41–51.

Neff, W. D., 1975: Quantitative evaluation of acoustic echoes from the planetary boundary layer. NOAA Tech. Rep., ERL 322-WPL 38, 34 pp. [Available from the author, NOAA Laboratories/WPL, Boulder, Colo. 80302 or Govt. Printing Office, Washington, D. C. 20402.]

Pennell, W. T., and M. A. LeMone, 1974: An experimental study of turbulence structure in the fair-weather, trade wind boundary layer. *J. Atmos. Sci.*, **31**, 1308–1323.

Rayment, R., 1973: An observational study of the vertical profile of the high frequency fluctuations of the wind in the atmospheric boundary layer. *Bound.-Layer Meteor.*, **3**, 284–300.

——, and C. J. Readings, 1974: A case study of the structure and energetics of an inversion. *Quart. J. Roy. Meteor. Soc.*, **100**, 221–233.

Readings, C. J., and H. E. Butler, 1972: The measurement of atmospheric turbulence from a captive balloon. *Meteor. Mag.*, **101**, 286–298.

——, D. A. Haugen and J. C. Kaimal, 1974: The 1973 Minnesota atmospheric boundary layer experiment. *Weather*, **29**, 309–312.

Richter, J. H., D. R. Jensen, V. R. Noonkester, T. G. Konrad, A. Arnold and J. R. Rowland, 1974: Clear air convection: A close look at its evolution and structure. *Geophys. Res. Lett.*, **1**, 173–176.

Rowland, J. R. and A. Arnold, 1975: Vertical velocity structure and geometry of clear air convection elements. *Preprints 16th Radar Meteorology Conf.*, 22–23 April, Houston, Tex., Amer. Meteor. Soc., 296–303.

Tennekes, H., 1970: Free convection in the turbulent Ekman layer of the atmosphere. *J. Atmos. Sci.*, **27**, 1027–1034.

——, 1975: Reply to comments on "A model for the dynamics of the inversions above a convective boundary layer." *J. Atmos. Sci.*, **32**, 992–995.

Smedman-Högström, A. S., and U. Högström, 1975: Spectral gap in surface layer measurements. *J. Atmos. Sci.*, **32**, 340 350.

Tsvang, L. R., 1969: Microstructure of temperature fields in the free atmosphere. *Radio Sci.*, **4**, 1175–1177.

Volkovitskaya, Z. I., and V. N. Ivanov, 1970: Turbulent energy dissipation in the atmospheric boundary layer. *Izv. Atmos. Ocean. Phys.*, **5**, 249–253.

Willis, G. E., and J. W. Deardorff, 1974: A laboratory model of the unstable planetary boundary layer. *J. Atmos. Sci.*, **31**, 1297–1307.

Wyngaard, J. C., 1975: Modeling the planetary boundary layer—extension to the stable case. *Bound.-Layer Meteor.*, **9**, 441–460.

——, and O. R. Coté, 1971: The budgets of turbulent kinetic energy and temperature variance in the atmospheric surface layer. *J. Atmos. Sci.*, **28**, 190–201.

——, and ——, 1974: The evolution of a convective planetary boundary layer—a higher-order-closure model study. *Bound.-Layer Meteor.*, **7**, 289–308.

——, ——, and Y. Izumi, 1971a: Local free convection, similarity, and the budgets of shear stress and heat flux. *J. Atmos. Sci.*, **28**, 1171–1182.

——, Y. Izumi and S. A. Collins, Jr., 1971b: Behavior of the refractive-index structure parameter near the ground. *J. Opt. Soc. Amer.*, **61**, 1646–1650.

——, O. R. Coté and K. S. Rao, 1974: Modeling the atmospheric boundary layer. *Advances in Geophysics*, Vol. 18A, Academic Press, 193–211.

Zilitinkevich, S. S., 1972: On the determination of the height of the Ekman boundary layer. *Bound.-Layer Meteor.*, **3**, 141–145.

——, 1975: Comments on "A model for the dynamics of the inversion above a convective boundary layer". *J. Atmos. Sci.*, **32**, 991–992.